LIMNOLOGY and OCEANOGRAPHY

ASLO

Limnol. Oceanogr. 67, 2022, 1760–1775

doi: 10.1002/lno.12165

Isotopic signatures of biotic and abiotic N_2O production and consumption in the water column of meromictic, ferruginous Lake La Cruz (Spain)

Jana Tischer,[1*] **Jakob Zopfi**,[1] **Claudia Frey**,[1] **Paul M. Magyar**,[1] **Andreas Brand**,[2,3] **Kirsten Oswald**,[2,3] **Corinne Jegge**,[2,4] **Caitlin H. Frame**,[1] **María R. Miracle**,[5,†] **Xavier Sòria-Perpinyà**,[5] **Eduardo Vicente**,[5] **Moritz F. Lehmann**[1]

[1]Department of Environmental Sciences, University of Basel, Basel, Switzerland
[2]Department of Surface Waters—Research and Management, EAWAG, Swiss Federal Institute of Aquatic Science and Technology, Kastanienbaum, Switzerland
[3]Institute of Biogeochemistry and Pollutant Dynamics, ETH Zurich, Swiss Federal Institute of Technology, Zurich, Switzerland
[4]School of Architecture, Civil and Environmental Engineering, EPFL, Swiss Federal Institute of Technology, Lausanne, Switzerland
[5]Department of Microbiology and Ecology, Cavanilles Institute of Biodiversity and Evolutionary Biology, University of Valencia, Burjassot, Spain

Abstract

Lakes can be important sources of the potent greenhouse gas nitrous oxide (N_2O) to the atmosphere, but to what extent abiotic processes may contribute to lacustrine N_2O production remains uncertain. We assessed pathways of N_2O production and reduction in the water column of meromictic and iron-rich Lake La Cruz, Spain, including chemodenitrification-induced N_2O formation via the reaction of reactive nitrogen (N) (e.g., NO_2^-) with ferrous iron (Fe [II]). In the oxic waters (~8–10 m), N_2O concentrations above atmospheric equilibrium were associated with comparatively low $\delta^{15}N\text{-}N_2O$, high $\delta^{15}N\text{-}NH_4^+$, and high N_2O ^{15}N-site-preference (SP) values (up to ~29‰), suggesting N_2O production by nitrification. N_2O concentrations were highest (23–33 nM) near the depth of oxygen depletion (~11–14.5 m), likely due to production by nitrifier denitrification and/or denitrification, as indicated by decreasing SP values (as low as 12‰). Further below (~14.5–17 m), N_2O consumption was indicated by increasing SP values and a $\delta^{18}O\text{-vs.-}\delta^{15}N$ relationship (1.8–2.9) typical for stand-alone N_2O reduction. The coupled N-vs.-O isotope signatures thus highlight the spatial, redox-dependent separation of incomplete and complete denitrification. In incubations with sterile-filtered lake water and ^{15}N-labeled or unlabeled substrate, NO_2^- was reduced by Fe^{2+} to N_2O, even at low nitrite concentrations (5 μM NO_2^-). In the water column, the spatial separation of NO_2^- and Fe (II) during our samplings appears to preclude elevated rates of chemodenitrification, but during periods of overlapping NO_2^- and Fe(II) in Lake La Cruz, and potentially in other lakes, its distinct N_2O $\delta^{18}O\text{-vs.-}\delta^{15}N$ relationship of ~1 : 1, as experimentally determined, could help to detect it.

*Correspondence: jana.tischer@unibas.ch

Additional Supporting Information may be found in the online version of this article.

Author Contribution Statement: J.Z. and M.F.L. conceived research project. J.T., M.F.L., and J.Z. conceptualized research and experimental design. J. T., J.Z., M.F.L., A.B., K.O., C.J., M.R.M., X.S.P., and E.V. contributed to the successful sampling campaigns and to the data acquisition of physicochemical parameters in the water column of Lake La Cruz. J.T. and C.H.F. carried out the stable isotope analysis. J.T. designed and conducted the lake water incubation experiments. J.T., C.F., C.H.F., J.Z. and M.F.L. carried out the data analysis. J.T. wrote the paper, with substantial input from M.F.L., C.F., C.H.F., P.M.M., and J.Z. All other authors approved the final version of the submitted manuscript.
[†]Deceased.

Nitrous oxide (N_2O) is a potent greenhouse gas and an important ozone-layer-depleting substance in the atmosphere (Wang et al. 1976; Ravishankara et al. 2009). Terrestrial ecosystems including inland waters are relevant sources of both natural and anthropogenic N_2O, but with a high uncertainty in their contribution to global N_2O emissions (Maavara et al. 2019). N_2O production in these ecosystems has been attributed primarily to microbially mediated nitrogen (N)-transforming processes (Tian et al. 2020). The relative contribution of abiotic N_2O production mechanisms is still a matter of debate, particularly in lakes.

The main microbial N_2O-producing processes are nitrification, nitrifier denitrification, and denitrification. During the first step of nitrification, where ammonia-oxidizing bacteria (AOB) and/or ammonia-oxidizing archaea (AOA) oxidize

ammonia (NH_3) or ammonium (NH_4^+) to nitrite (NO_2^-) via hydroxylamine (NH_2OH), and nitric oxide (NO) (Schreiber et al. 2012; Kozlowski et al. 2016), N_2O can be produced as a side product via several pathways. Non-enzymatic N_2O production may be attributed to the autoxidation of NH_2OH (Fig. 1, pathway 1; Moews and Audrieth 1959), the reaction between NH_2OH and NO both derived from NH_3 (Fig. 1, pathway 2; Bonner et al. 1978), or a hybrid mechanism, where one NH_3-derived N atom (e.g., NH_2OH) and one NO_2^--derived N atom form one N_2O molecule (Fig. 1, pathway 3; Döring and Gehlen 1961). In AOB, N_2O is thought to be produced primarily biologically through NO reduction by a yet unknown enzyme (Fig. 1, pathway 4; Schreiber et al. 2012). At relatively low oxygen (O_2) levels, AOB respire NO_2^- by reduction to NO and N_2O (Fig. 1, pathway 5) via nitrifier denitrification (review in Wrage et al. 2001). A different subset of microorganisms carries out denitrification, the stepwise enzymatic reduction of nitrate (NO_3^-) to NO_2^-, NO, N_2O, and eventually to dinitrogen gas (N_2) (Fig. 1, pathway 6), under anaerobic and very low-O_2 conditions (Wrage et al. 2001). Abiotic N_2O production may occur via chemodenitrification, the reduction of NO_2^- (and possibly NO_3^-), with reduced iron (Fe(II); Fig. 1, pathway 7; Burgin and Hamilton 2007 and references therein). It can be accelerated by surface catalysts, such as mineral surfaces (Buchwald et al. 2016; Grabb et al. 2017), or dead bacterial detritus (Visser et al. 2020), and therefore indirectly connected to microbial activity, as microbes provide reactive N metabolites and catalyzing surfaces.

Process-specific isotope characteristics can help to trace N_2O cycling processes that occur in close proximity in natural environments. One valuable diagnosing tool in this regard is the isotopic offset, here defined as the isotopic difference between the initial source and the final product during N_2O production ($\Delta\delta^{15}N = \delta^{15}N_{source} - \delta^{15}N_{product}$ and $\Delta\delta^{18}O = \delta^{18}O_{source} - \delta^{18}O_{product}$, respectively), where the N and O isotopic composition of N_2O and its precursor compounds are reported in the conventional delta-notation of per mil (‰) units, that is, $\delta^{15}N$ or $\delta^{18}O$ values (Toyoda et al. 2015). Typical isotopic differences for N-transformation processes are presented in Fig. 1. For instance, they may help to identify AOB-associated N_2O production from ammonium via nitrification

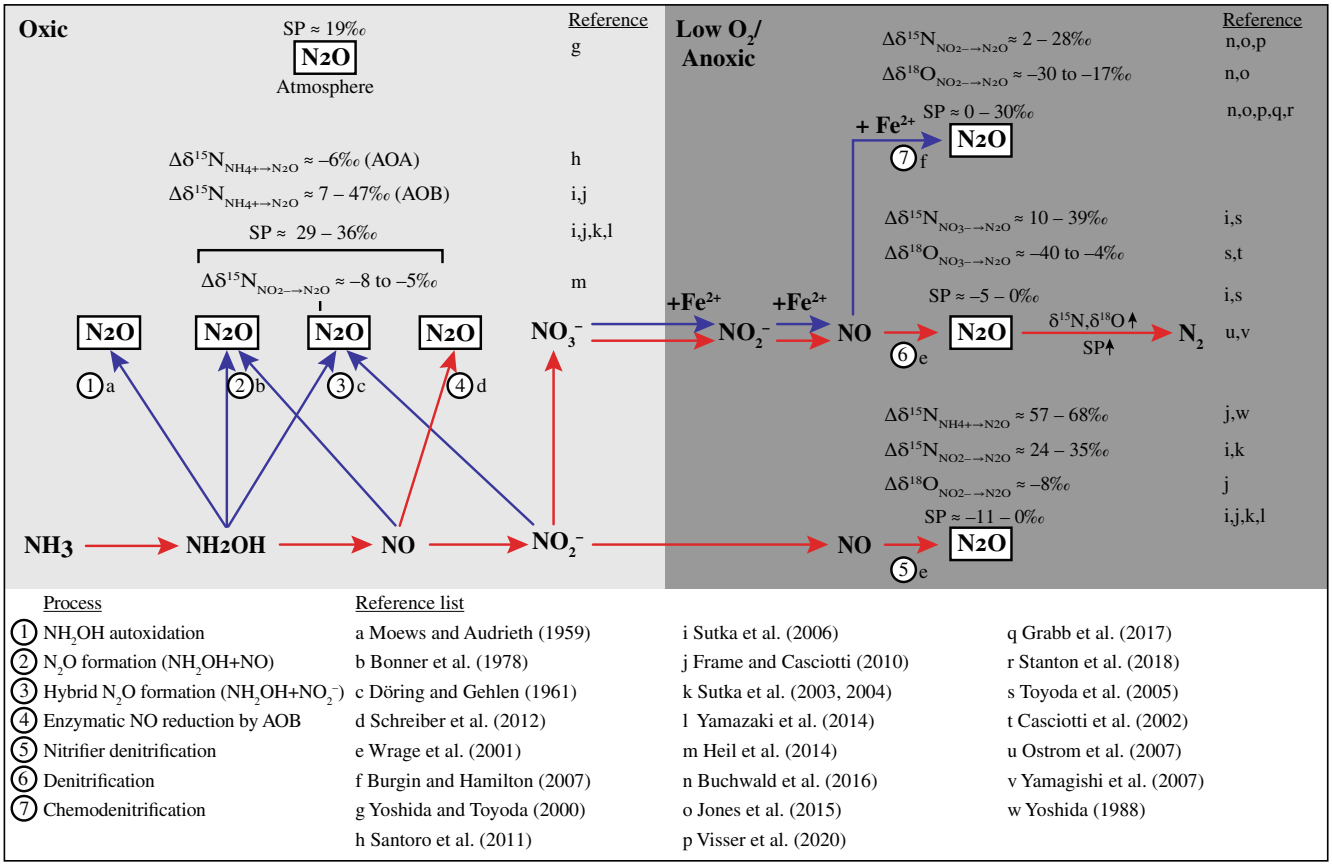

Fig. 1. Environmentally relevant enzymatic and non-enzymatic reactions that produce or consume N_2O, including typical N_2O SP values and characteristic isotope fractionation effects ($\Delta\delta^{15}N \approx \delta^{15}N_{substrate} - \delta^{15}N_{product}$, $\Delta\delta^{18}O \approx \delta^{18}O_{substrate} - \delta^{18}O_{product}$). Red arrows represent enzymatic reactions; blue arrows represent non-enzymatic reactions. Processes relevant in oxic environments are included in the light gray box; processes most relevant in low-O_2 and anoxic environments are in the dark gray box. *See* the text for more information.

($\Delta\delta^{15}N_{NH4+\rightarrow N2O} \approx 7‰$) and nitrifier denitrification ($\Delta\delta^{15}N_{NH4+\rightarrow N2O} \approx 57‰$) (Frame and Casciotti 2010). Contrarily, the N and O isotopic offsets with nitrite or nitrate as substrate can hardly distinguish between denitrification ($\Delta\delta^{15}N_{NO3-\rightarrow N2O} \approx 10–39‰$, $\Delta\delta^{18}O_{NO3-\rightarrow N2O} \approx -40$ to $-4‰$; Casciotti et al. 2002; Toyoda et al. 2005; Sutka et al. 2006) and chemodenitrification ($\Delta\delta^{15}N_{NO2-\rightarrow N2O} \approx 2–30‰$, $\Delta\delta^{18}O_{NO2-\rightarrow N2O} \approx -30$ to $-17‰$; Jones et al. 2015; Buchwald et al. 2016; Visser et al. 2020).

The $\delta^{18}O$-vs.-$\delta^{15}N$ relationship of N_2O may be particularly helpful in constraining N_2O sources and sinks in low O_2/anoxic environments. While denitrification produces variable slopes in a $\delta^{18}O$-vs.-$\delta^{15}N$ space, for example, $\Delta\delta^{18}O : \Delta\delta^{15}N$ values between ~ -1.5 and 2.5 (Casciotti et al. 2002; Toyoda et al. 2005), N_2O consumption via denitrification results in a robust $\Delta\delta^{18}O : \Delta\delta^{15}N$ value of ~2.6 (Yamagishi et al. 2007; Ostrom and Ostrom 2012). At the same time, chemodenitrification produces N_2O with a relatively narrow range of $\Delta\delta^{18}O : \Delta\delta^{15}N$ values between ~0.7 and 1 (Jones et al. 2015; Visser et al. 2020).

The intramolecular ^{15}N distribution within N_2O, or site preference (SP), defined as the difference in the relative abundance of ^{15}N in the central (α) and terminal (β) N atoms in N_2O ($SP = \delta^{15}N^{\alpha} - \delta^{15}N^{\beta}$), provides information on the production pathway independent of the substrate N isotopic composition (Toyoda and Yoshida 1999). For example, the SP can distinguish between nitrification-associated N_2O formation with high SP values (> 29‰) and nitrifier denitrification and denitrification with relatively low values (< 0–10‰) (*see* Fig. 1). N_2O produced by abiotic reactions of NO_2^- or NO and Fe(II) displays highly variable SP values between 0 and 30‰ (Grabb et al. 2017; Visser et al. 2020).

Iron-rich meromictic lakes are considered potential modern analogs for ferruginous ancient oceans and represent valuable model ecosystems to study biogeochemical processes involving iron (Walter et al. 2014; Camacho et al. 2017). Abiotic interactions between the iron and the N cycle have been demonstrated in laboratory experiments and studied in natural environments including soils, marine sediments, and Antarctic lakes and ponds (Venterea 2007; Peters et al. 2014; Wankel et al. 2017). Clear evidence for such abiotic interaction is lacking in lake water columns, despite the abundance and significance of boreal iron-rich shield lakes (Schiff et al. 2017). Chemodenitrification, for instance, may occur in ferruginous lakes like Lake Matano (Indonesia), Kabuno Bay (Democratic Republic of the Kongo) or Lake La Cruz (Spain), where Fe(II)-oxidizing, nitrate-reducing bacteria, which are known to catalyze abiotic NO_2^- reduction, have been identified (Walter 2011; Kopf et al. 2013; Michiels et al. 2017). In this study, we use a multifaceted isotope geochemical approach to investigate the N_2O dynamics in meromictic, ferruginous Lake La Cruz. We combine (i) water column hydrochemical measurements, including the analysis of the stable isotope composition and SP of dissolved N_2O; (ii) ^{15}N-isotope label incubation experiments to identify and quantify N_2O production pathways; and (iii) experiments to determine the isotope effects during the abiotic reaction between NO_2^- and Fe^{2+} to form N_2O, as a prerequisite to identify this process potentially occurring in the lake. We assess the applied isotopic approaches in the context of their value in determining the relative importance and spatial partitioning of different N_2O sources and sinks in the water column of Lake La Cruz. Furthermore, we aim at verifying whether under the ferruginous conditions in Lake La Cruz, chemodenitrification can be an important contributor to ecosystem-scale N_2O production.

Methods

Field site

Lake La Cruz is located in the Iberian Ranges near the city of Cuenca, Spain, at an altitude of ~1000 m above sea level. It is a circular carbonate karstic sinkhole with a mean diameter of 132 m and a maximum depth of ~20 m (Vicente and Miracle 1988). The lake has been meromictic for more than 300 yr, due to a density gradient, which constitutes the chemocline, approximately 5 m above the lake bottom. The chemical stratification is mainly due to the high concentrations of calcium and magnesium bicarbonate ions in the permanent monimolimnion. High concentrations of other ions, including NH_4^+ and dissolved Fe^{2+}, additionally contribute to the water column stability (Rodrigo et al. 2001; Walter et al. 2014). Lake La Cruz is a closed lake, and the total depth, as well as the position of the redox transition zone (RTZ, here defined as the layer between the depth, where the O_2 concentration reaches < 5 μM and the first depth of detectable sulfide (H_2S)) vary depending on the precipitation regime (Rodrigo et al. 2001).

In situ profiling and sample collection

We carried out two field campaigns, one in the first week of March 2015 and one in the third week of March 2017. Hydrocasts were performed at the deepest point in the center of the lake (39°59′20″N, 01°52′25″W). As described in Oswald et al. (2016), a profiling in situ analyzer (PIA), equipped with a multi-parameter probe, as well as light (PAR; LI-193 Spherical Underwater Quantum Sensor, LI-COR) and chlorophyll a (Chl *a*; ECO-FL, Wetlands, EX/EM = 470/695) sensors was used to measure conductivity, turbidity, temperature, depth (pressure), pH, photosynthetically active radiation, Chl *a*, and H_2S. Furthermore, two micro-optodes (PSt1 and TOS7, PreSens) attached to the PIA were used to detect dissolved O_2 concentrations down to 125 and 20 nM, respectively (Kirf et al. 2014). A battery-driven peristaltic pump was used for sample collection, whereby the outlet of an air-tight tubing (PVC Solaflex, Maagtechnic) was directly attached to the PIA, allowing sampling from precisely known depths. Unfiltered water was fixed with monobromobimane for H_2S analysis (Fahey and Newton 1987). To avoid O_2 contamination, we filled a 120-mL serum vial and let the water overflow one volume before pipetting water from the bottom of the vial

directly into a tube prepared with the fixing reagent. For total iron concentrations, we took unfiltered water samples by filling 60-mL plastic syringes with water and subsequently fixed the water in HNO_3 (~150 mM final concentration). For the analysis of dissolved Fe concentrations, we filtered water through 0.2-μm syringe filters and fixed it in ~150 mM HNO_3. For the analysis of NO_3^-, NO_2^-, NH_4^+, and sulfate (SO_4^{2-}) concentrations, and for the isotope analysis of NO_x (NO_3^- and NO_2^-)/nitrate, we filtered aliquots of water through a 0.45 μm syringe filter [Correction added on 23 June 2022, after first online publication: "NO_x" changed to read "NO_x (NO_3^- and NO_2^-)". Also corrected μM to μm.]. In the nitrate isotope samples, nitrite was removed using sulfamic acid (Granger and Sigman 2009). H_2S, NO_x/nitrate isotope, and ammonium isotope samples were kept frozen; all other samples were stored at 4°C prior to analysis. For N_2O analyses, we collected samples in 160-mL serum bottles, and poisoned them immediately with 5 mL 10 M NaOH. Subsequently, a 1-mL headspace was introduced, and the vials were sealed with 20 mm gray butyl stoppers (VWR), shaken vigorously, and stored cold and dark until analysis. For incubation experiments in 2017, water from 8 and 14.5 m depth was pumped directly into sterile borosilicate glass bottles and sterile 10-L plastic canisters.

Solute and metal concentrations

NO_3^-, NO_2^-, NH_4^+, and N_2O—Photometrical methods involving phenol and sulfanilamide and the Griess reagent (naphtalethylenediamine dihydrochloride) were used to measure NH_4^+ and NO_2^-, respectively (Hansen and Koroleff 1999). NO_x was analyzed by reduction to NO in an acidic vanadium(III) (V^{3+}) solution followed by chemiluminescence detection of the NO (Antek Model 745; Braman and Hendrix 1989). NO_3^- concentrations were calculated as the difference of NO_x and NO_2^- concentrations. Dissolved N_2O concentrations were determined by isotope-ratio mass spectrometry (IRMS) (*see* below).

Fe—In 2015, total and dissolved Fe concentrations were measured by inductively coupled plasma-mass spectrometry (ICP-MS, Spectro Ciros Vision) and in 2017 by inductively coupled plasma optical emission spectrometry (ICP-OES, Agilent Technologies). Concentrations of particulate iron were calculated as the difference of total and dissolved iron.

H_2S, SO_4^{2-}—H_2S was analyzed using high-performance liquid chromatography (HPLC, Dionex) with fluorescence detection (Zopfi et al. 2008). SO_4^{2-} was quantified by ion chromatography (940 Professional IC Vario, Metrohm).

Stable isotopes of nitrogen species

N_2O—Using helium (He) as carrier gas, N_2O was purged from the sample vials into a customized purge-and-trap system (McIlvin and Casciotti 2010), and analyzed by continuous-flow IRMS (GC-IRMS). CO_2 was trapped via Ascarite II and remaining traces additionally separated from N_2O in the GC column (RT®-Q-BOND, 30 m, RESTEK, 25°C), resulting in baseline-separated peaks of CO_2 and N_2O. Measured N_2O isotope ratios were calibrated against N_2O injected from a reference N_2O tank (≥ 99.9986%, Messer) calibrated on the Tokyo Institute of Technology scale (Mohn et al. 2012) by J. Mohn (EMPA, Switzerland) for bulk and site-specific isotopic composition. Ratios of m/z 45/44, 46/44, and 31/30 signals were converted to $\delta^{15}N$-N_2O (referenced to AIR), $\delta^{18}O$-N_2O (referenced to Vienna Standard Mean Ocean Water, VSMOW), and site-specific $\delta^{15}N^{\alpha}$ and $\delta^{15}N^{\beta}$-N_2O according to Frame and Casciotti (2010), with an additional three-point correction (Mohn et al. 2014) using measurements of three isotopic mixtures of N_2O in synthetic air (CA06261: $\delta^{15}N = -35.74 \pm 0.07$‰, $\delta^{15}N^{\alpha} = -22.21 \pm 0.39$‰, $\delta^{15}N^{\beta} = -49.28 \pm 0.40$‰, $\delta^{18}O = 26.94 \pm 0.23$‰, Fl.53504: $\delta^{15}N = 48.09$‰, $\delta^{15}N^{\alpha} = 1.71$‰, $\delta^{15}N^{\beta} = 94.44$‰, $\delta^{18}O = 36.10$‰, and CA08214: $\delta^{15}N = 6.84$‰, $\delta^{15}N^{\alpha} = 17.11$‰, $\delta^{15}N^{\beta} = -3.43$‰, $\delta^{18}O = 35.39$‰; kindly provided by J. Mohn). A final correction step was included to correct for the difference between gaseous and aquatic samples/standards by subtracting the values of measured atmospheric N_2O equilibrated in water from the expected isotope values of atmospheric N_2O using values reported in Yoshida and Toyoda (2000).

N_2O concentrations were analyzed by calibrating the total peak areas in water column samples with N_2O standards of known concentrations (2015: air and standards prepared with the denitrifier method, *see* next paragraph; 2017: isotope standard CA06261). The N_2O concentrations in the water column at equilibrium with the atmosphere were calculated based on Weiss and Price (1980), taking into account water temperature and salinity. Atmospheric partial pressures of N_2O were taken from the NOAA/ESRL halocarbons in situ program (http://www.esrl.noaa.gov/gmd/).

NO_x, NO_3^-, and NH_4^+—NO_x and NO_3^- isotope ratios were analyzed using the denitrifier method (Sigman et al. 2001; Casciotti et al. 2002; McIlvin and Casciotti 2010). Briefly, after the bacterial conversion of NO_x or NO_3^- to N_2O, the N_2O was analyzed using the customized purge-and-trap system and continuous-flow GC-IRMS described before. NO_3^- isotopes were calibrated against the international NO_3^- standards IAEA-N3 ($\delta^{15}N = 4.7$‰, $\delta^{18}O = 25.6$) and USGS34 ($\delta^{15}N = -1.8$‰, $\delta^{18}O = -27.9$‰), and an internal standard (UBN-1; $\delta^{15}N = 14.15$‰, $\delta^{18}O = 25.7$‰). The N and O isotopic composition of nitrite in incubation experiments was determined by the reduction of NO_2^- to N_2O with sodium azide, followed by GC-IRMS analysis (McIlvin and Altabet 2005). Isotopic calibration was performed by concurrent analysis of the international NO_2^- standards N7373 ($\delta^{15}N = -79.6$‰, $\delta^{18}O = 4.5$‰) and N10219 ($\delta^{15}N = 2.8$‰, $\delta^{18}O = 88.5$‰). Finally, ammonium N isotope ratios were determined by the conversion of NH_4^+ to NO_2^- with hypobromite, followed by the transformation of the NO_2^- to N_2O with sodium azide (Zhang et al. 2007) and its isotopic analysis as described above. The NH_4^+-derived N_2O N isotope ratios were first referenced against the international NO_2^- standards N7373 and N10219, and in a second

step against the international NH_4^+ standards IAEA-N1 ($\delta^{15}N = 0.43‰$) and IAEA-N2 ($\delta^{15}N = 20.41‰$), which underwent the same processing as the samples. All N and O isotopic data are reported on the per mil (‰) scale referenced to AIR and VSMOW, respectively: $\delta^{15}N = ([^{15}N]/[^{14}N])_{Sample}/[^{15}N]/[^{14}N]_{AIR} - 1) \times 1000‰$, and $\delta^{18}O = ([^{18}O]/[^{16}O]_{Sample}/[^{18}O]/[^{16}O]_{VSMOW} - 1) \times 1000‰$.

^{15}N-label incubation experiments

Potential N_2O production rates in the presence or absence of dissolved Fe^{2+} were determined in incubation experiments with ^{15}N-labeled substrates under different redox conditions ("Exp_oxic $^{15}N_2O$" and "Exp_anoxic $^{15}N_2O$"). Incubation conditions and added substrates are summarized in Supporting Information Table S1. For all abiotic treatments, lake water was filter-sterilized with 0.2-μm cyclopore track-edged membrane filters (Whatman). For experiments with oxic water from 8 m depth, ^{15}N-tracers were added to a volume of 2 L in canisters (either 5 μM $^{15}NO_2^-$ at ambient NH_4^+ concentrations of ~40 μM, or 40 μM $^{15}NH_4^+$ + 5 μM unlabeled NO_2^-) from sterile 2–5 mM stock solutions (99% ^{15}N-NH_4Cl or ≥ 98% ^{15}N-$NaNO_2$; Cambridge Isotope Laboratories, Inc.). The water was distributed into 160-mL serum vials without a headspace and closed with butyl rubber stoppers and aluminum seals. For anoxic experiments with water from 14.5 m water depth, we purged the water in 2-L borosilicate bottles with He for 30 min before adding 5 μM of the respective ^{15}N-tracer, and, in some of the treatments, 10 μM dissolved Fe^{2+}. At this sampling depth, no ambient Fe had been detected. We added ^{15}N-tracers from 2 mM stock solutions (99% ^{15}N-KNO_3, or ≥ 98% ^{15}N-$NaNO_2$; Cambridge Isotope Laboratories, Inc.), and unlabeled NO_2^- and Fe^{2+} as solutions of $NaNO_2$ and $FeSO_4$, respectively. The water was anoxically transferred without leaving headspace into He-purged 160-mL serum vials already closed with butyl rubber stoppers and aluminum seals using an adjusted protocol from Holtappels et al. (2011). Both oxic and anoxic incubation bottles were incubated at ~16°C in the dark. At each of three preassigned time points (~12, 24, and 36 h), three bottles were sacrificed by introducing a 40-mL He headspace and terminating microbial activity, as well as potential chemodenitrification by adding 5 mL of 10 M NaOH, which precipitates ferrous iron and strongly decreases the reactivity of nitrite (Braida and Ong 2000; Visser et al. 2020). One bottle was sacrificed directly after starting the experiment. The water samples were sterile-filtered and stored frozen. NO_2^-, NO_3^-, and NH_4^+ concentrations were measured as described above. The total N_2O in each incubation bottle was analyzed for concentration and m/z ion ratios 45/44 and 46/44 as described for natural abundance stable isotope measurements of water column N_2O samples. For highly ^{15}N-enriched N_2O samples, we reduced the resistance on the m/z 46 detector from 1×10^{11} Ω to 1×10^9 Ω, to yield a 100-fold lower amplification of the $^{15}N^{15}N^{16}O$ signal. Some highly enriched ^{15}N samples were measured with a too high resistance and therefore excluded from analysis. The raw data were corrected for linearity effects of the sample size/peak area on the 45/44 and 46/44 ratios through the analysis of N_2O standards with different amounts of N_2O. $^{44}N_2O$ was determined as described above for the N_2O concentration analysis of the in situ water samples. Masses $^{45}N_2O$ and $^{46}N_2O$ were then calculated based on the 46/44 and 45/44 ratios. Production rates of exogenous, endogenous, and total N_2O were determined using equations described in Trimmer et al. (2016) (*see* Supporting Information Appendix S1). Exogenous N_2O is produced entirely from the ^{15}N-labeled substrate added, considering the ^{15}N fraction in the substrate pool, while endogenous N_2O mixes one N atom from the ^{15}N-labeled substrate and a second from another N-molecule in the incubation. Possible N isotope pairing outcomes for the oxic incubations are visualized in Supporting Information Fig. S1. The rates of N_2O production were calculated based only on the linear increase in $^{44}N_2O$, $^{45}N_2O$, and $^{46}N_2O$, to exclude plateauing N species concentrations due to a terminated abiotic reaction and artifacts due to bottle effects mostly towards the end of the incubations. We estimated the detection limit as 1.5-times the standard error (SE) of the rates. The consumption of the ^{15}N-tracers was calculated based on the temporal change of the respective N substrate concentration, multiplied with the ^{15}N atom fraction, using the same timepoints as for the N_2O rate determination. NO_2^- production rates in the NO_3^--amended treatments were calculated analogously. A *t*-test was performed to test whether the rates were significant. N_2O yields were calculated as (i) as the ratio of the ^{15}N-tracer consumption rate vs. the total N_2O production rate and (ii) as the ratio of produced N_2O vs. produced N_2 (*see* below) in the anoxic incubations. The production of $^{15}NH_4^+$ was determined via chemical conversion to $^{15}N_2$ using hypobromite (Risgaard-Petersen et al. 1995) and subsequent analysis of ^{15}N-N_2 by IRMS as described in Robertson et al. (2016). Parallel ^{15}N-label incubation experiments were conducted in 2017 to determine N_2 production rates ("Exp $^{15}N_2$"), using an adjusted protocol described in Wenk et al. (2016) (*see* Supporting Information Appendix S2; Table S2).

Abiotic experiment with NO_2^- and Fe^{2+}

Concentration and isotope dynamics of chemodenitrification were determined experimentally ("Exp_chemo"). Lake water from 14.5 m depth was filtered through 0.2-μm membrane filters (Whatman), filled into sterile 20-mL serum vials, and closed airtight with rubber stoppers. The water was purged for 10 min, leaving a He headspace, before amending each vial with NO_2^- and subsequently with Fe^{2+} from sterile and anoxic stock solutions of $NaNO_2$ and $FeSO_4$, respectively, in exchange with the headspace volume (i.e., leaving no headspace). The pH during the experiment was 9.34 ± 0.14. Target concentrations were 100 μM NO_2^- and 200 μM Fe^{2+}. At each of the seven time points between 0 and 48 h (t_0–t_6), three samples were sacrificed by taking 8 mL of the sample solution, replacing it

with He, and adding 0.5 mL 10 M NaOH. From the 8 mL sample, aliquots for NO_2^- concentration measurements were fixed and analyzed as described above and samples for Fe^{2+} were fixed in sulfamic acid (40 mM final concentration) and analyzed using the ferrozine assay (Stookey 1970; Klueglein and Kappler 2013). Aliquots for NO_2^- isotopes were filtered through 0.2-μm syringe filters, and frozen immediately at −80°C. After thawing, the samples were analyzed with the azide method (*see* above). Using the serum vials, we determined the N_2O concentrations and isotope ratios as described above for the water column N_2O isotope analyses.

Results

Geochemical conditions in Lake La Cruz

The water column of Lake La Cruz during our sampling campaigns can be divided into the oxic water column, the anoxic hypolimnion, and the deep permanently anoxic monimolimnion, where the RTZ consists of the lower oxic water column (<5 μM O_2) and the upper anoxic hypolimnion (Supporting Information Fig. S2). The oxic water column includes the photosynthetically most active zone, at 7–8 m, as indicated by a local Chl *a* maximum (Supporting Information Fig. S3b). O_2 was completely consumed at ~14 m in 2015 and at ~12 m in 2017 (Fig. 2a). Strong changes in pH from ~8.5 (2015) and ~8.7 (2017) in the oxic water column, to ~6.3 (2015) and ~6.6 (2017) below ~15.5–17 m water depth mark the chemocline that separates the anoxic hypolimnion from the monimolimnion underneath (Fig. 2b). Paralleling the pH profile, conductivity increased from ~400 μS cm^{-1} in the chemocline to >1000 μS cm^{-1} in the bottom waters (Supporting Information Fig. S3c).

Below the RTZ, total Fe was dominated by dissolved Fe, with maximum concentrations of ~300 μM in near-bottom waters (Fig. 2d). Particulate Fe concentrations were highest at the RTZ and in the anoxic water, but at comparatively low concentrations < 2 μmol L^{-1} (Fig. 2e; Supporting Information Fig. S2). H_2S accumulated in the deep anoxic water column below 15 m with up to ~20 μM (Fig. 2j), whereas SO_4^{2-} decreased to < 10 μM in the monimolimnion (Supporting Information Fig. S3f).

N-species concentrations in the water column

The most abundant inorganic N compound throughout the water column was NH_4^+, with concentrations increasing from ~20 μM in the oxic epilimnion to almost 5 mM in the monimolimnion (Fig. 2h). NO_3^- concentrations fluctuated around 3 μM (2015) and 5 μM (2017) in the oxic water, with a minor concentration peak at 8 m in both years, and decreased

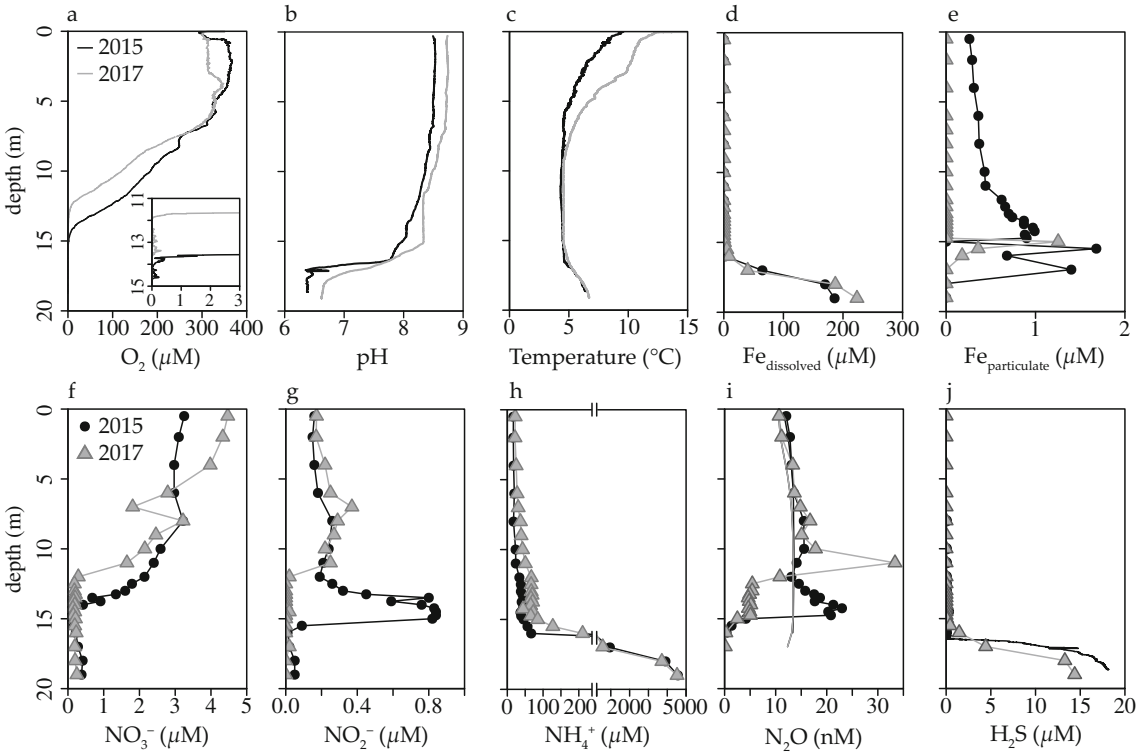

Fig. 2. Physicochemical profiles from March 2015 and March 2017 in Lake La Cruz. (**a**) O_2 and trace O_2 (insert), (**b**) pH, (**c**) temperature, (**d**) dissolved Fe concentration, (**e**) particulate Fe concentration, (**f**) NO_3^- concentration, (**g**) NO_2^- concentration, (**h**) NH_4^+ concentration, (**i**) N_2O concentration, and (**j**) H_2S concentration. Water column profile data of O_2, pH, temperature, Fe (particulate), NO_3^-, and NO_2^- from 2015 have been published previously in Oswald et al. (2016).

sharply at the RTZ to values below 0.5 μM (Fig. 2f; Supporting Information Fig. S2). NO_2^- was present in the epilimnion at low concentrations of ~0.2–0.4 μM, with a subtle peak at 7–10 m in both years, but only in 2015 with a clear nitrite maximum (0.8 μM) in the RTZ (Fig. 2g; Supporting Information Fig. S2). The N_2O concentration profiles revealed a subtle N_2O oversaturation of ~2 nM above equilibrium concentration in a discernible water layer at 8–10 m (up to 13.6 nM in 2015, and up to 16.7 nM in 2017, Fig. 2i). N_2O concentrations were highest at 12–14.5 m (23.0 nM), near the depth of O_2 depletion, in 2015. In 2017, the N_2O maximum (33.4 nM) was somewhat higher in the water column, at 11 m, where O_2 was still ~40 μM (Fig. 2i; Supporting Information Fig. S2). Below 16 m, N_2O concentrations were below the detection limit.

Isotopic compositions of N-species in the water column

The $\delta^{15}N$ values of N_2O in the surface water were close to those of atmospheric N_2O. With increasing N_2O oversaturation, at ~8–10 m, the $\delta^{15}N$-N_2O values decreased (Fig. 3b). In 2015, the increasing N_2O concentrations between 12.0 and 15.5 m were accompanied by decreasing $\delta^{15}N$-N_2O values from 2.2 to −1.1‰ and by increasing $\delta^{15}N$-NO_x values from ~8 to ~22‰ (Supporting Information Fig. S4a), resulting in a $\Delta\delta^{15}N_{NOx\rightarrow N2O}$ value of ~23‰ at the depth of maximum N_2O concentration. In 2017, the $\delta^{15}N$-N_2O values increased slightly towards the concentration peak, from −3.2 to −0.8‰. Further below, they continued to increase to final values of 6–8‰ (Fig. 3b). $\delta^{15}N$-NH_4^+ values (measured only in 2017) were highest in the oxic water column at 6–7 m with 15–16‰ and decreased with increasing NH_4^+ concentrations through the RTZ to a robust value of 3‰ in the bottom waters (Fig. 3e). $\delta^{18}O$-N_2O values were more or less invariant at ~45‰ within the oxic epilimnion, close to atmospheric N_2O. They increased with increasing depth and plateaued at ~65‰ (2015) and at ~85‰ (2017) in the RTZ (Fig. 3c). The $\delta^{18}O$-NO_3^- values in the oxic water column ranged mostly between 16 and 20‰ (Supporting Information Fig. S4c) with a $\Delta\delta^{18}O_{NO3\rightarrow N2O}$ value of −37‰ at the depth of maximum N_2O concentration. N_2O SP values increased from atmospheric values in the surface waters to 24.7‰ in 2015 and to 28.5‰ in 2017 at the layer of oxic N_2O oversaturation (7–8 m; Fig. 3d). With the drop in N_2O concentrations at ~15 m depth in 2015, N_2O SP values increased again. In 2017, the SP systematically decreased between the oxic N_2O maximum and the second N_2O maximum to a value of 13.0‰, and then increased again to 20.0‰ with decreasing N_2O concentrations (Fig. 3d).

N_2O production and reduction potential

The results from the ^{15}N-N_2O production experiments (Exp_oxic $^{15}N_2O$ and Exp_anoxic $^{15}N_2O$) are shown in Fig. 4 and Supporting Information Table S3. In the oxic unfiltered, that is, microbially active, incubation experiments, N_2O production rates were relatively low but significant. The addition of $^{15}NH_4^+$ and non-labeled NO_2^- led to higher total N_2O production rates ($16.7 \pm 2.1 \times 10^{-3}$ nmol-N_2O L^{-1} d^{-1}, $p < 0.001$, $n = 10$) than the sole addition of $^{15}NO_2^-$ ($9.5 \pm 3.9 \times 10^{-3}$ nmol-N_2O L^{-1} d^{-1}, $p < 0.05$, $n = 10$). The percentage of endogenous (above-expected mass 45) N_2O production (Fig. 4a) was lower in the $^{15}NH_4^+$ treatment (44%) than in the $^{15}NO_2^-$ treatment (78%).

N_2O production in the anoxic incubations was several orders of magnitude higher than the oxic N_2O production rates. In the experiments with $^{15}NO_3^-$ (Fig. 4b), the rates of ^{15}N transformation were highest in the $^{15}NO_3^-$-only treatment (356.5 ± 56.8 nmol-N_2O L^{-1} d^{-1}, $p < 0.01$, $n = 4$). In the $^{15}NO_3^- + Fe^{2+}$ treatment, the rate was significantly lower (185.7 ± 30.7 nmol-N_2O L^{-1} d^{-1}, $p < 0.001$, $n = 9$). In the filtered $^{15}NO_3^- + Fe^{2+}$ treatment, N_2O production was significant (35.9 ± 11.2 nmol-N_2O L^{-1} d^{-1}, $p < 0.01$, $n = 8$) compared to the control without Fe^{2+} (rate below detection limit). In both unfiltered incubations with $^{15}NO_3^-$, some N_2O was observed to be consumed toward the last timepoint (~1.5 d), at least in some of the bottles (Supporting Information Fig. S5e). In the $^{15}NO_2^-$-amended experiments (Fig. 4c), N_2O production was

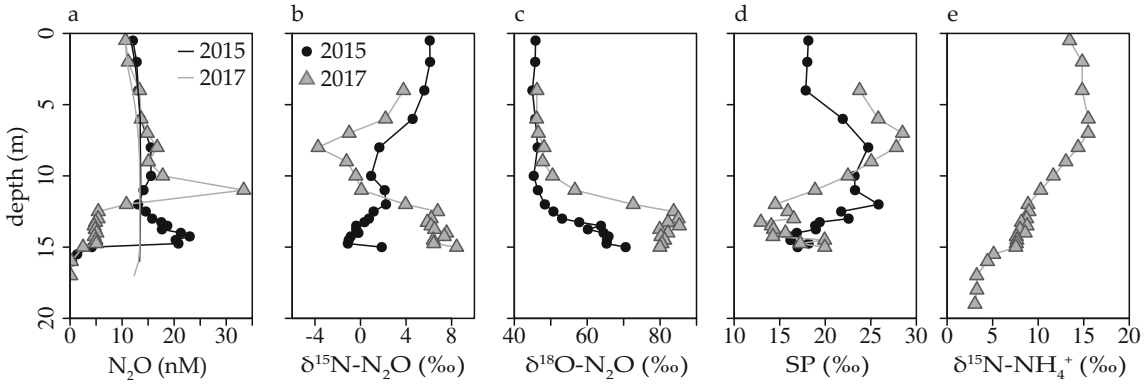

Fig. 3. N_2O concentration and N-species isotope profiles from March 2015 and March 2017 in Lake La Cruz. (**a**) N_2O concentration, the lines indicate the N_2O concentration expected for atmospheric equilibration, (**b**) $\delta^{15}N$-N_2O, (**c**) $\delta^{18}O$-N_2O, (**d**) N_2O SP, and (**e**) $\delta^{15}N$-NH_4^+.

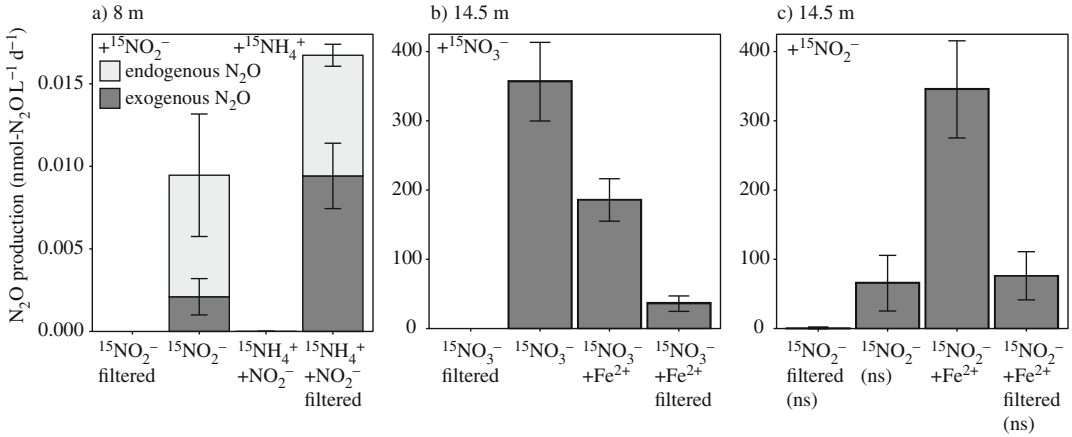

Fig. 4. N_2O production rates in incubation experiments performed with ^{15}N-labeled substrates in March 2017. (**a**) Oxic incubations in 8 m depth with $^{15}NO_2^-$ and $^{15}NH_4^+$ tracer (Exp_oxic $^{15}N_2O$). (**b**) Anoxic incubations in 14.5 m depth with $^{15}NO_3^-$ tracer, and **c)** anoxic incubations in 14.5 m depth with $^{15}NO_2^-$ tracer (Exp_oxic $^{15}N_2O$). Non-significant production slopes above detection limit are indicated by "ns." Error bars indicate standard error of replicate means of the total N_2O production. Exogenous N_2O is produced solely via the ^{15}N-labeled substrate, taking into account the ^{15}N-fraction in the substrate pool. Endogenous N_2O originates from one ^{15}N-tracer molecule and one ambient ^{14}N-molecule of a different substrate, hence it can help to distinguish between N_2O production pathways. For details, *see* "Methods" section and Supporting Information Fig. S1. Note the different scale in (**a**).

highest when Fe^{2+} was added to the unfiltered sample (345.4 ± 70.1 nmol-N_2O L^{-1} d^{-1}, $p < 0.01$, $n = 6$). N_2O production was similar in the unfiltered $^{15}NO_2^-$-only treatment (65.5 ± 40.2 nmol-N_2O L^{-1} d^{-1}, $p = 0.082$, $n = 6$) and in the filtered treatment with $^{15}NO_2^- + Fe^{2+}$ (76.2 ± 34.8 nmol-N_2O L^{-1} d^{-1}, $p = 0.080$, $n = 3$). In the abiotic incubations with added Fe^{2+}, we neither observed a production of ^{15}N-NH_4^+ (Exp_anoxic $^{15}N_2O$; Supporting Information Table S3) nor of $^{30}N_2$ and $^{29}N_2$ (Exp $^{15}N_2$; Supporting Information Table S2). N_2O vs. N_2 production ratios in the unfiltered incubations from Exp_anoxic $^{15}N_2O$ and Exp $^{15}N_2$, respectively, were up to ~250% (Supporting Information Table S2).

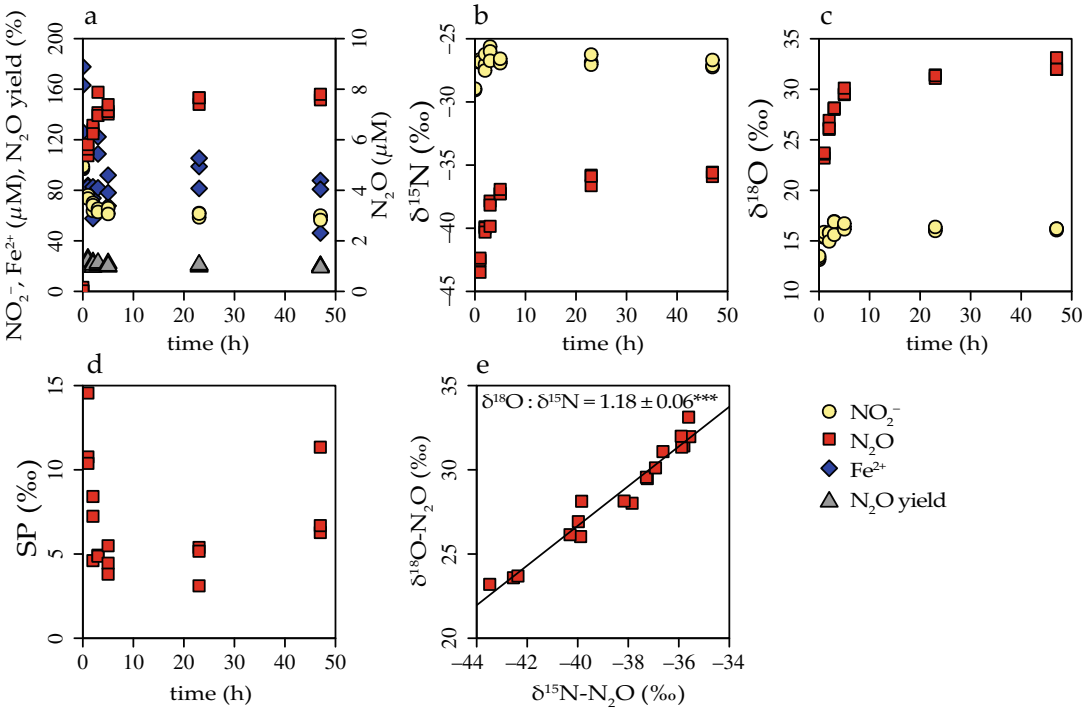

Fig. 5. Concentration and isotope dynamics during the abiotic reduction of NO_2^- with Fe^{2+} (Exp_chemo). (**a**) Concentrations of NO_2^- and Fe^{2+}, (**b**) $\delta^{15}N$ of NO_2^- and product N_2O, (**c**) $\delta^{18}O$ of NO_2^- and product N_2O, (**d**) site preference (SP) of product N_2O, and **(e)** $\delta^{18}O$ vs. $\delta^{15}N$ of N_2O.

NO_2^- and N_2O isotope dynamics of chemodenitrification in incubation experiments

The NO_2^- and N_2O concentration and isotope dynamics during the incubation with unlabeled NO_2^- (Exp_chemo) are summarized in Fig. 5 and Supporting Information Fig. S6. During the reduction of NO_2^- coupled to the oxidation of Fe^{2+}, NO_2^- decreased from ~100 to ~60 μM, and Fe^{2+} from ~155 to ~75 μM within the first 5 h after adding the substrates. Hence, NO_2^- and Fe^{2+} decreased with a stochiometric ratio of ~1 : 2.2, which is close to the expected ratio of 1 : 2 for chemodenitrification reactions with N_2O as only N-product, but somewhat higher than the ratio of 1 : 1.4 when assuming that 75% of the NO_2^- is transformed into NO and only 25% into N_2O (*see* equations in Supporting Information Table S4). N_2O reached maximum concentrations of 7.7 μM (Fig. 5a). The molar N_2O yields, that is, the N_2O produced relative to the NO_2^- consumed, were 20% to 25% throughout the experimental period. After ~3 h, the reaction slowed down and finally stalled, although none of the substrates were consumed to completion. The $\delta^{15}N$-N_2O values increased from −42.8 initially to −35.7‰ at the end of the incubation (Fig. 5b), as expected for closed-system dynamics. The $\delta^{18}O$-N_2O values increased in parallel with the $\delta^{15}N$-N_2O from 23.5 to 32.4‰ (Fig. 5c). The O : N isotope enrichment ratio for N_2O was 1.18 ± 0.06 SE (Fig. 5e). During the reactive part of the abiotic experiment, N_2O SP values decreased, starting at t_1 (N_2O concentrations at t_0 were too low for N_2O isotope and SP analysis), from 11.9 to 4.5‰, before rising to an average endpoint value of 8.1‰. The overall average SP was 6.9 ± 3.1‰ (Fig. 5d). The $\delta^{15}N$ and $\delta^{18}O$ values of NO_2^- increased within the first 5 h from −29.0 to −26.8‰ and from 13.3 to 16.2‰, respectively, and then stabilized at this value (Fig. 5b,c). Isotope effects of nitrite are presented and discussed in Supporting Information Appendix S4.

Discussion

Biogeochemical processes in the water column

In the oxic water column, at 7–8 m, the photosynthetically most active zone coincided with elevated NO_3^- and NO_2^- concentrations, indicating that photosynthesis as well as ammonium and nitrite oxidation occur in close vicinity. In the RTZ, decreasing nitrate concentrations, and accumulating nitrite in 2015, indicate active denitrification or dissimilatory nitrate reduction to ammonium.

The generally low sulfate load in Lake La Cruz explains the high concentrations of dissolved Fe in the monimolimnion, because only minor FeS precipitation takes place, exporting iron to the sediment (Rodrigo et al. 2001; Walter et al. 2014). Clear evidence for microbial Fe(II) oxidation coupled to nitrate reduction in the summer has been reported by Walter (2011). The results from our samplings in spring show dissolved Fe concentrations declining to zero-level still below the depth of maximum NO_3^- consumption, suggesting that Fe is not the prime reductant for NO_3^-. Fe oxidation can also be coupled to biotic or abiotic nitrite reduction (i.e., nitrite chemodenitrification). At least in March 2015, the dissolved Fe gradient seems to be associated with the nitrite gradient at the bottom of the secondary nitrite maximum. Yet, the relative concentrations of dissolved Fe in the monimolimnion (several hundreds of μM) vs. those of nitrite within the nitrite maximum (< 1 μM), require that, if at all, chemodenitrification is fueled by a cryptic nitrite (and potentially nitrate) cycle, that is, the close coupling of the production of nitrite by nitrate-reducing bacteria and consumption by Fe-dependent nitrite reduction (*see* below), without great net accumulation of nitrite.

N_2O production in the oxic water column

A zone of active enzymatic and/or non-enzymatic N_2O production associated to nitrification was identified at ~8–10 m depths, where N_2O concentrations were ~2 nM above atmospheric equilibrium. The depletion in ^{15}N in N_2O, the concomitant enrichment of ^{15}N in the substrate NH_4^+ pool, as well as the increase in N_2O SP to 25–27‰ are strong indicators for nitrification. On the other hand, the isotopic offset between substrate NH_4^+ and product N_2O ($\Delta\delta^{15}N_{NH4+\rightarrow N2O} \approx$ 18‰) did not allow us to identify N_2O production pathways, since the observed value fell between the expected values for nitrification and nitrifier denitrification (Frame and Casciotti 2010).

The oxic ^{15}N-tracer incubation experiments provided some evidence for the activity of nitrifier denitrification, especially in the $^{15}NO_2^-$ tracer incubations, where 22% of produced N_2O was derived from two ^{15}N-tracer molecules. Furthermore, the production of endogenous N_2O in the incubations with added $^{15}NH_4^+$ indicates hybrid N_2O formation and other non-enzymatic or enzymatic N_2O production pathways. A detailed discussion of the isotopic constraints on N_2O production in the oxic water column is available in Supporting Information Appendix S3.

Identifying the dominant N_2O production pathways in the RTZ

We argue that the N_2O concentration peaks at the depths of O_2 depletion mainly had a biological origin, despite the potential for chemodenitrification demonstrated in the abiotic incubation experiments (Exp_anoxic $^{15}N_2O$ and Exp_chemo, *see* discussion below). Denitrification appears as the most likely N_2O source in 2015, as indicated by the consumption of NO_3^- just below the depth of O_2 depletion, concurrent with the production of NO_2^- and N_2O, while, to some extent, nitrifier denitrification might contribute. The biological production of up to ~500 nmol $^{30}N_2$ L^{-1} d^{-1} in unfiltered incubations with amended $^{15}NO_x$ (Exp $^{15}N_2$) confirms the activity of denitrifying microorganisms. In 2017, the highest N_2O concentration was observed above the RTZ at ~110 μM O_2 (11 m), suggesting that at that time nitrifier denitrification was the

prime N_2O source, as it tolerates higher O_2 concentrations than canonical denitrification (Zhu et al. 2013; Babbin et al. 2014). Furthermore, a still relatively high NO_3^- concentration of 1.7 μM at 11 m indicates that the depth of nitrate consumption via denitrification was below the N_2O peak.

The N_2O concentration peak in 2015 was accompanied by N isotope effects between the substrate NO_x and the produced N_2O ($\Delta\delta^{15}N_{NOx\rightarrow N2O}$ of 23‰) in the range of previously reported isotope offsets for denitrification ($\Delta\delta^{15}N_{NO3-\rightarrow N2O}$ = 10–39‰, Fig. 1) and nitrifier denitrification ($\Delta\delta^{15}N_{NO2-\rightarrow N2O}$ = 24–35‰, Fig. 1). For $\delta^{18}O$, the observed $\Delta\delta^{18}O_{NO3\rightarrow N2O}$ isotope effect of −37‰ in 2017 was at the lower end of the range of values reported for denitrification-derived N_2O ($\Delta\delta^{18}O$ = −40 to −4‰; Fig. 1). The negative isotopic offset for oxygen is due to O-isotope branching, that is, the selective release of ^{16}O during N_2O formation and the preferential remaining of ^{18}O within the N_2O bond. A contribution to N_2O production by canonical denitrification and/or nitrifier denitrification is also indicated by the decreasing N_2O SP values to ~16‰ (2015) and 13‰ (2017), respectively, at the depth of maximum N_2O accumulation. Still, the intermediate SP values (i.e., between the endmember values of nitrification and denitrification) suggest that nitrification-associated N_2O production still plays a role with regards to the RTZ SP signature. Increasing SP values in the deepest, anoxic N_2O samples to 20‰ (2017) indicate partial N_2O reduction. Chemodenitrification with an SP between 5 and 12‰ (Exp_chemo) could have an impact on the observed intermediate SP values but, as we argue below mainly based on the dissolved Fe and NO_2^- concentration profiles, its contribution in the RTZ is likely negligible.

Interestingly, in other O_2-deficient environments, N_2O concentration peaks were typically associated with high SP values, for example, in the Black Sea with values up to 46.5‰ (Westley et al. 2006), in Lake Lugano North Basin with up to 25.7‰, and in Lake Lugano South Basin with up to 42.3‰ (Wenk et al. 2016). There, denitrification was assumed to be important, and the high SP was seen as a result of overprinting isotope effects by nitrification or N_2O reduction. The relatively low SP values in the RTZ of Lake La Cruz may result from a sluggish transfer of high-SP N_2O from the oxic water column compared to other lakes, potentially due to high water column stability, and a lack of effective mixing between the oxic N_2O maximum and the N_2O peak at the oxic-anoxic interface.

A high N_2O production potential by denitrification was confirmed in the ^{15}N-label incubation experiments at 14.5 m with $^{15}NO_3^-$, where 356.5 nmol-N_2O L^{-1} d^{-1} was produced with a parallel accumulation of NO_2^- (Exp_anoxic $^{15}N_2O$). Yields of produced N_2O vs. produced N_2 of 13% to 249% show that in some of the biologically active incubations, the accumulation of N_2O can exceed the production of N_2. We point out that high N_2O : N_2 yields are uncommon in freshwater (e.g., in a reservoir, in situ N_2O : N_2 ratios were much lower, < 20%; Beaulieu et al. 2014). Yet, the accumulation of N_2O from incomplete denitrification was likely only temporary, as indicated by the reduction of N_2O at the last timepoint in the ^{15}N-NO_3^- treatment.

The slopes of $\delta^{18}O$-vs.-$\delta^{15}N$-N_2O plots in the RTZ represent yet another useful tool to assign water layers in the RTZ, where either N_2O production or N_2O reduction is dominant, allowing us to further corroborate the different N_2O production/consumption niches in the water column. We can pinpoint a zone of dominant N_2O production via denitrification between 12 and 15 m in 2015, where we observed a negative N_2O $\Delta\delta^{18}O$: $\Delta\delta^{15}N$ slope of −6.2 (Fig. 6). Within the RTZ, the $\delta^{15}N$-N_2O values decrease simultaneously with increasing N_2O concentrations and decreasing NO_x concentrations (i.e., complete consumption at ~15.5 m), and NO_x becomes enriched in ^{15}N with continuous substrate consumption, as expected for denitrification. Contrarily, $\delta^{18}O$-N_2O values increase as a consequence of Rayleigh distillation and the branching ^{18}O isotope effect during N_2O production. As to what extent the observed $\delta^{18}O$: $\delta^{15}N$ slope in N_2O also reflects N_2O reduction is difficult to say but the net decreasing $\delta^{15}N$ values indicate the dominance of N_2O production over N_2O reduction. A stronger contribution from N_2O reduction would be expected to drive the $\delta^{15}N$-N_2O to higher values (Ostrom et al. 2007; Yamagishi et al. 2007). In 2017, the $\Delta\delta^{18}O$: $\Delta\delta^{15}N$ slope between 10 and 12 m, where N_2O concentrations reach a maximum, is less conclusive with regards to identifying a specific water layer where N_2O production is dominating, as our

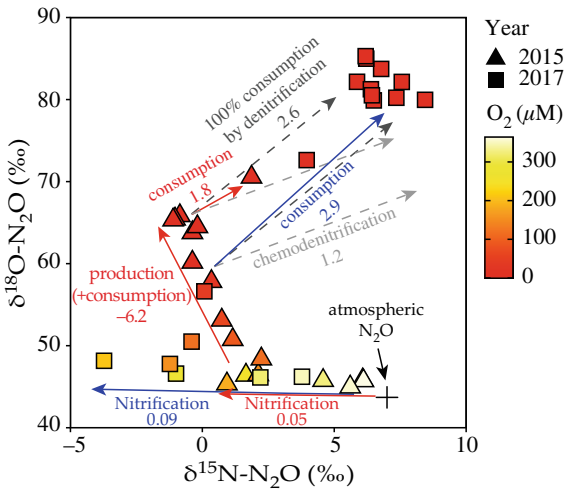

Fig. 6. Dual N- and O-isotope signatures of N_2O in the water column of Lake La Cruz. The solid-line arrows represent measured $\Delta\delta^{18}O$: $\Delta\delta^{15}N$ trends, and the interpretation of these trends in the context of specific N_2O producing/consuming processes in 2015 (red) or 2017 (blue). The dashed-line arrows including numbers indicate experimentally determined $\delta^{18}O$: $\delta^{15}N$ slopes of isolated processes: 100% consumption via denitrification (dark gray; Ostrom and Ostrom 2012) and chemodenitrification (light gray, this study).

sampling scheme did not cover these depths in detail. In both years, the $\Delta\delta^{18}O : \Delta\delta^{15}N$ trends (1.8 in 2015 and 2.9 in 2017) associated with decreasing N_2O concentrations (15–15.5 m in 2015 and 11–13 m in 2017) indicate that N_2O reduction dominates the N_2O isotopic signature, with little contribution from simultaneous gross N_2O production. That is, these ratios are relatively close to the theoretical value of pure N_2O reduction ($\delta^{18}O : \delta^{15}N \approx 2.6$; Yamagishi et al. 2007; Ostrom and Ostrom 2012). The difference between the 2 years may possibly be attributed to the varying impact of chemodenitrification in these water layers (*see* discussion below). We highlight that the analysis of $\delta^{18}O$-vs.-$\delta^{15}N$-N_2O plots could be especially helpful in water columns, where N_2O concentration peaks do not correspond to $\delta^{15}N$ and $\delta^{18}O$ extrema of N_2O, and hence, the identification of N_2O production and reduction processes is more difficult.

Chemodenitrification and associated isotope effects

Evidence for potential chemodenitrification

Fe-amended ^{15}N-incubation experiments with water from 14.5 m water depth show a marked potential for chemodenitrification (Exp_anoxic $^{15}N_2O$), suggesting that it could contribute to total N_2O production in Lake La Cruz. For the first time, we provide evidence of chemodenitrification in experiments conducted with natural lake water, as opposed to previous studies investigating chemodenitrification in an artificial matrix (Jones et al. 2015; Buchwald et al. 2016). Thermodynamic calculations confirm that the reaction of Fe^{2+} and NO_2^- is not only favorable under the conditions in the incubation experiments but also under in situ conditions, even at nanomolar substrate concentrations (Supporting Information Tables S4, S5). In the incubations, N_2O production stalled within 12 h, even though both NO_3^-/NO_2^- and Fe^{2+} were still present. We speculate that the reaction terminated due to accumulation of the intermediate NO (Kampschreur et al. 2011), inhibiting the reduction of NO_2^-. NO reduction to N_2O, in turn, depends on the dynamics of gas equilibrium and can be impeded by the accumulation of N_2O (Visser et al. 2020).

In the unfiltered $^{15}NO_2^-$ incubation experiments with Fe^{2+}, we observed a relatively high N_2O production rate, whereas in both the filtered $NO_2^- + Fe^{2+}$ (no cells and particles) experiment and in the unfiltered NO_2^--only (biological denitrification) experiment N_2O production was just above detection limit, suggesting that reactive surfaces of bacterial or other cells and/or particulate iron catalyze the reaction of Fe^{2+} with NO_2^-. This effect has been previously demonstrated in various experiments under controlled lab conditions (Sutka et al. 2006; Kopf et al. 2013; Visser et al. 2020). In experiments with NO_3^- and Fe^{2+}, we did not observe catalyzing effects of reactive surfaces on N_2O production as they were possibly masked by microbial N_2O production through denitrification. Yet, although nitrite-driven chemodenitrification seemed to be the most important abiotic N_2O production process, N_2O production in the filtered $NO_3^- + Fe^{2+}$ treatment clearly occurred as well. Chemodenitrification of nitrate with Fe may be an underappreciated nitrate reduction process in natural environments, competing with the enzymatic nitrate reduction, at least in iron-rich settings such as Lake La Cruz.

Isotopic signatures during experimental chemodenitrification

The distinct in vitro isotope signature of Fe-coupled chemodenitrification, imparted on the N_2O pool (Exp_chemo), provides a basis for interpreting community N and O isotope effects in the water column (next subsection). The SP values in our experiment with an average of 6.9 ± 3.1‰ are within the broad range of previously reported values for chemodenitrification between 0 and 30‰ (Buchwald et al. 2016; Visser et al. 2020). These highly variable SP values are likely due to the impact of intermediates such as NO or nitrosyl ($Fe[NO]^+$), which are, in turn, influenced by the environmental conditions (Buchwald et al. 2016). A more detailed discussion on the SP dynamics during experimental chemodenitrification can be found in Supporting Information Appendix S5.

In contrast to the observed overall spread for SP, the coupled N and O isotope effect during N_2O production by chemodenitrification yielded a constant $\Delta\delta^{18}O : \Delta\delta^{15}N$ trend of 1.18 ± 0.06. This value is similar to, but somewhat higher than, values observed by Jones et al. (2015) and Visser et al. (2020), who reported $\delta^{18}O$-N_2O vs. $\delta^{15}N$-N_2O data from chemodenitrification experiments that correspond to slopes on $\delta^{18}O$-vs.-$\delta^{15}N$-N_2O plots between ~0.7 and 1.0. Our experiments with natural lake water thus expand the existing evidence that N_2O production by chemodenitrification displays coupled dual N_2O N/O isotope signatures that are distinct from microbial processes such as N_2O reduction, which displays a robust ratio of 2.6 (Yamagishi et al. 2007; Ostrom and Ostrom 2012).

Chemodenitrification in the water column

The concentration profiles of N- and Fe-compounds in Lake La Cruz revealed a relatively thin water layer (15 m depth in 2015, 12–15 m depth in 2017), where chemodenitrification is most likely to occur, with N_2O accumulation and presence of traces of dissolved Fe and NO_2^-. However, we point out that at least in spring 2017, based on the spatial separation of NO_2^- and dissolved iron between 12 and 15 m depth, chemodenitrification does most likely not play a major role for N_2O production in these depths. In contrast, below the N_2O maximum in 2015, where N_2O was reduced completely, chemodenitrification is more likely to have occurred, considering the nitrite and dissolved Fe concentration profiles. Here, particulate Fe accumulation indicates active Fe(II) oxidation to Fe(III). In our incubations (Exp_anoxic $^{15}N_2O$, Exp_chemo), the fractional N_2O yield of chemodenitrification reached values of 20–30%, independent

of the initial substrate concentrations, and we thus expect similar yields in the water column of Lake La Cruz. When assuming concentrations of 0.5 μM for overlapping NO_2^- and Fe(II), which may possibly apply to the situation in 2015, an N_2O yield of 25% with respect to NO_2^- reduction would result in 125 nM N_2O produced. Yet, we observed rather low concentrations of N_2O in the respective water layer (< 5 nM). In such a situation, chemodenitrification (i.e., its typical biogeochemical signature of high N_2O production with respect to N_2) could be hidden because active denitrification, as we have demonstrated, prevents N_2O from accumulating.

Theoretically, N_2O SP measurements allow identifying, or excluding, chemodenitrification, but we argue that two fundamental problems preclude the reliable use of SP for the detection of chemodenitrification in the RTZ of Lake La Cruz with SP values of 13–16‰. First, it is unclear whether the SP values around 5–12‰ determined in our incubation experiment (Exp_chemo) are representative for the SP values of N_2O produced in situ. Since NO concentrations only reach very low concentrations in natural water bodies (Tian et al. 2019 and references therein), as compared to the incubation experiment, where NO probably accumulated, reaction dynamics and SP effects could be different. Second, a single two-endmember SP approach cannot be applied, since contributions from canonical and/or nitrifier denitrification, simultaneous N_2O reduction via denitrification, and remnant relict N_2O from aerobic N_2O production above the RTZ all shape the SP values within the RTZ. The SP minima of 16‰ (2015) and 13‰ (2017) are in fact similar to the SP values expected for chemodenitrification, but these values likely reflect a mixed signal of nitrification and denitrification rather than chemodenitrification. In the zone below the N_2O maxima/SP minima, which is the most likely water depth for chemodenitrification to occur based on the geochemical profiles, SP values increase up to 20‰, which is higher than the expected SP of 5–12‰ for chemodenitrification. We suspect N_2O reduction to be the driving process here (*see* above). Generally, the large uncertainties of the SP associated to N_2O produced via chemodenitrification does not make it a suitable indicator to trace this process in the environment.

We turn to the dual N and O isotope trends of N_2O to potentially disentangle chemodenitrification and microbial denitrification (Fig. 6). The $\Delta\delta^{18}O : \Delta\delta^{15}N$ value of 1.8 for the deepest data points in 2015 falls in-between the theoretical expected trends for 100% N_2O reduction via denitrification (2.6; Yamagishi et al. 2007; Ostrom and Ostrom 2012) and chemodenitrification (1.2, Exp_Chemo), respectively, possibly representing a combined chemodenitrification/microbial N_2O reduction signal. In 2017, decreasing N_2O concentrations below the N_2O peak at ~11–12.5 m were associated to a $\Delta\delta^{18}O : \Delta\delta^{15}N$ ratio of 2.9 pointing toward a layer of N_2O reduction without significant contribution of chemodenitrification, as this value is close to the theoretical value of 2.6 for microbial denitrification. This seems plausible, as during the sampling in 2017 the spatial separation between NO_x- and Fe(II)-containing waters was much more pronounced. In turn, this implies that chemodenitrification undergoes inter- and/or intra-annual fluctuations, probably modulated by seasonal/inter-annual changes in water column biogeochemistry. For example, higher Chl *a* concentrations in 2017 indicate a larger input of organic compounds to fuel canonical denitrification. Based on the apparent specificity of the dual N- and O-isotope ratio of N_2O, the coupled N-vs.-O N_2O isotope measurements were more useful than the SP analyses for identifying chemodenitrification.

Although the monimolimnion of Lake La Cruz displays high dissolved iron concentrations, Fe-coupled chemodenitrification was likely responsible for only a minor percentage of the total N_2O observed in the RTZ. Incubation experiments revealed, however, that chemodenitrification has the potential to contribute to N_2O production as much as canonical denitrification. For example, in winter, when the upper water column is well mixed and the depth of O_2 depletion is located at greater depth, NO_x and dissolved Fe profiles are more likely to overlap, and with higher concentrations, chemodenitrification may play a more important role in the overall N_2O production within the RTZ. Furthermore, the mixing of the upper water column could cause the transport of N_2O from the RTZ to the upper water column and eventually to the atmosphere.

Conclusions

We present a comprehensive tool set based on different stable isotopic approaches to investigate biotic and abiotic N_2O production pathways in aquatic environments. We demonstrate that profiles of N_2O concentration and the isotopic characteristics of N_2O ($\delta^{15}N$, $\delta^{18}O$, and SP) are valuable indicators of nitrification-associated N_2O production, N_2O production via nitrifier denitrification and/or canonical denitrification, as well as N_2O reduction via denitrification, in different compartments of Lake La Cruz. In particular, the coupled N_2O N-vs.-O isotope signatures highlight the redox-dependent transition from incomplete and complete denitrification in the water column. Incubation experiments with lake water and amended ^{15}N-tracers proved useful for a more quantitative assessment of the above-mentioned processes. For example, $^{15}NO_3^-$ incubations confirmed high rates of N_2O production in the near bottom oxygen-deficient waters.

In addition to traditional microbial processes, we assessed the potential contribution of chemodenitrification to N_2O production in Lake La Cruz. Lake water incubations with high N_2O yields during the reaction between NO_2^- and Fe^{2+}, even at low substrate concentrations, suggest that chemodenitrification rates could be relevant under the observed in situ conditions in the water column. However, the identification of in situ gross N_2O production by chemodenitrification is intricate, as it is likely overprinted by microbial N_2O reduction. Most promising with regard to detecting chemodenitrification in the water column is the analysis of the N_2O $\delta^{18}O$ vs. $\delta^{15}N$, as the $\Delta\delta^{18}O : \Delta\delta^{15}N$ ratio seems typical for chemodenitrification

(~1 : 1.2 in this study), that is, distinct from biological isotope effects. Periods of overlapping availability of NO_x and iron in the anoxic hypolimnion of Lake La Cruz may transiently lead to a substantial increase in N_2O production via chemodenitrification, and N_2O $\Delta\delta^{18}O : \Delta\delta^{15}N$ values could be deployed to detect this.

N_2O produced via chemodenitrification may not only be relevant in Lake La Cruz or other meromictic, iron-rich lakes, but potentially also in seasonally stratified lakes, which accumulate dissolved iron in the temporarily anoxic water column. For example, numerous boreal shield lakes can develop an anoxic hypolimnion with high dissolved iron concentrations in summer (Schiff et al. 2017), possibly providing suitable conditions for chemodenitrification during stratification and N_2O release to the atmosphere during mixing. Furthermore, in the context of ferruginous and anoxic ancient oceans, our findings imply that large amounts of the potent greenhouse gas N_2O generated via chemodenitrification might have contributed to an ice-free Mesoproterozoic Ocean (Stanton et al. 2018).

Data availability statement

Data are available through the PANGAEA data repository at https://www.pangaea.de (Tischer et al. 2022, doi:10.1594/PANGAEA.943248).

References

Babbin, A. R., R. G. Keil, A. H. Devol, and B. B. Ward. 2014. Organic matter stoichiometry, flux, and oxygen control nitrogen loss in the ocean. Science **344**: 406–408. doi:10.1126/science.1248364

Beaulieu, J. J., R. L. Smolenski, C. T. Nietch, A. Townsend-Small, M. S. Elovitz, and J. P. Schubauer-Berigan. 2014. Denitrification alternates between a source and sink of nitrous oxide in the hypolimnion of a thermally stratified reservoir. Limnol. Oceanogr. **59**: 495–506. doi:10.4319/lo.2014.59.2.0495

Bonner, F. T., L. S. Dzelzkalns, and J. A. Bonucci. 1978. Properties of nitroxyl as intermediate in the nitric oxide-hydroxylamine reaction and in trioxodinitrate decomposition. Inorg. Chem. **17**: 2487–2494. doi:10.1021/ic50187a030

Braida, W., and S. K. Ong. 2000. Decomposition of nitrite under various pH and aeration conditions. Water Air Soil Pollut. **118**: 13–26. doi:10.1023/A:1005193313166

Braman, R. S., and S. A. Hendrix. 1989. Nanogram nitrite and nitrate determination in environmental and biological materials by vanadium(III) reduction with chemiluminescence detection. Anal. Chem. **61**: 2715–2718. doi:10.1021/ac00199a007

Buchwald, C., K. Grabb, C. M. Hansel, and S. D. Wankel. 2016. Constraining the role of iron in environmental nitrogen transformations: Dual stable isotope systematics of abiotic NO_2-reduction by Fe(II) and its production of N_2O. Geochim. Cosmochim. Acta **186**: 1–12. doi:10.1016/j.gca.2016.04.041

Burgin, A. J., and S. K. Hamilton. 2007. Have we overemphasized the role of dentitrification in aquatic ecosystems? A review of nitrate removal pathways. Front. Ecol. Environ. **5**: 89–96 doi:10.1890/1540-9295(2007)5[89:HWOTRO]2.0.CO;2

Camacho, A., X. A. Walter, A. Picazo, and J. Zopfi. 2017. Photoferrotrophy: Remains of an ancient photosynthesis in modern environments. Front. Microbiol. **8**: 1–17. doi:10.3389/fmicb.2017.00323

Casciotti, K. L., D. M. Sigman, M. G. Hastings, J. K. Böhlke, and A. Hilkert. 2002. Measurement of the oxygen isotopic composition of nitrate in seawater and freshwater using the denitrifier method. Anal. Chem. **74**: 4905–4912. doi:10.1021/ac020113w

Döring, C., and H. Gehlen. 1961. Über die Kinetik der Reaktion zwischen Hydroxylamin und Salpetriger Säure. Z. Anorg. Allg. Chem. **312**: 32–44. doi:10.1002/zaac.19613120106

Fahey, R. C., and G. L. Newton. 1987. Determination of low-molecular-weight thiols using monobromobimane fluorescent labeling and high-performance liquid chromatography. Methods Enzymol. **143**: 85–96. doi:10.1016/0076-6879(87)43016-4

Frame, C. H., and K. L. Casciotti. 2010. Biogeochemical controls and isotopic signatures of nitrous oxide production by a marine ammonia-oxidizing bacterium. Biogeosciences **7**: 2695–2709. doi:10.5194/bg-7-2695-2010

Grabb, K. C., C. Buchwald, C. M. Hansel, and S. D. Wankel. 2017. A dual nitrite isotopic investigation of chemodenitrification by mineral-associated Fe(II) and its production of nitrous oxide. Geochim. Cosmochim. Acta **196**: 388–402. doi:10.1016/j.gca.2016.10.026

Granger, J., and D. M. Sigman. 2009. Removal of nitrite with sulfamic acid for nitrate N and O isotope analysis with the denitrifier method. Rapid Commun. Mass Spectrom. **23**: 3753–3762. doi:10.1002/rcm.4307

Hansen, H. P., and F. Koroleff. 1999. Determination of nutrients, p. 159–228. *In* K. Grasshoff, K. Kremling, and M. Ehrhardt [eds.], Methods of seawater analysis. Wiley-VCH. doi:10.1002/9783527613984.ch10

Heil, J., B. Wolf, N. Brüggemann, L. Emmenegger, B. Tuzson, H. Vereecken, and J. Mohn. 2014. Site-specific ^{15}N isotopic signatures of abiotically produced N_2O. Geochim. Cosmochim. Acta **139**: 72–82. doi:10.1016/j.gca.2014.04.037

Holtappels, M., G. Lavik, M. M. Jensen, and M. M. M. Kuypers. 2011. ^{15}N-labeling experiments to dissect the contributions of heterotrophic denitrification and anammox to nitrogen removal in the OMZ waters of the ocean, p. 223–251. *In* M. G. Klotz [ed.], Methods in enzymology, v. **486**. Elsevier Inc. doi:10.1016/B978-0-12-381294-0.00010-9

Jones, L. C., B. Peters, J. S. Lezama Pacheco, K. L. Casciotti, and S. Fendorf. 2015. Stable isotopes and iron oxide mineral products as markers of chemodenitrification. Environ. Sci. Technol. **49**: 3444–3452. doi:10.1021/es504862x

Kampschreur, M. J., R. Kleerebezem, W. W. J. M. de Vet, and M. C. M. van Loosdrecht. 2011. Reduced iron induced nitric oxide and nitrous oxide emission. Water Res. **45**: 5945–5952. doi:10.1016/j.watres.2011.08.056

Kirf, M. K., C. Dinkel, C. J. Schubert, and B. Wehrli. 2014. Submicromolar oxygen profiles at the oxic–anoxic boundary of temperate lakes. Aquat. Geochem. **20**: 39–57. doi:10.1007/s10498-013-9206-7

Klueglein, N., and A. Kappler. 2013. Abiotic oxidation of Fe(II) by reactive nitrogen species in cultures of the nitrate-reducing Fe(II) oxidizer *Acidovorax* sp. BoFeN1—questioning the existence of enzymatic Fe(II) oxidation. Geobiology **11**: 180–190. doi:10.1111/gbi.12019

Kopf, S. H., C. Henny, and D. K. Newman. 2013. Ligand-enhanced abiotic iron oxidation and the effects of chemical versus biological iron cycling in anoxic environments. Environ. Sci. Technol. **47**: 2602–2611. doi:10.1021/es3049459

Kozlowski, J. A., M. Stieglmeier, C. Schleper, M. G. Klotz, and L. Y. Stein. 2016. Pathways and key intermediates required for obligate aerobic ammonia-dependent chemolithotrophy in bacteria and Thaumarchaeota. ISME J. **10**: 1836–1845. doi:10.1038/ismej.2016.2

Maavara, T., R. Lauerwald, G. G. Laruelle, N. J. Bouskill, P. Van Cappellen, and P. Regnier. 2019. Nitrous oxide emissions from inland waters: Are IPCC estimates too high? Glob. Chang. Biol. **25**: 473–488. doi:10.1111/gcb.14504

McIlvin, M. R., and M. A. Altabet. 2005. Chemical conversion of nitrate and nitrite to nitrous oxide for nitrogen and oxygen isotopic analysis in freshwater and seawater. Anal. Chem. **77**: 5589–5595. doi:10.1021/ac050528s

McIlvin, M. R., and K. L. Casciotti. 2010. Fully automated system for stable isotopic analyses of dissolved nitrous oxide at natural abundance levels. Limnol. Oceanogr. Methods **8**: 54–66. doi:10.4319/lom.2010.8.54

Michiels, C. C., and others. 2017. Iron-dependent nitrogen cycling in a ferruginous lake and the nutrient status of Proterozoic oceans. Nat. Geosci. **10**: 217–222. doi:10.1038/NGEO2886

Moews, P. C., and L. F. Audrieth. 1959. The autoxidation of hydroxylamine. J. Inorg. Nucl. Chem. **11**: 242–246. doi:10.1016/0022-1902(59)80250-5

Mohn, J., B. Tuzson, A. Manninen, N. Yoshida, S. Toyoda, W. A. Brand, and L. Emmenegger. 2012. Site selective real-time measurements of atmospheric N_2O isotopomers by laser spectroscopy. Atmos. Meas. Tech. **5**: 1601–1609. doi:10.5194/amt-5-1601-2012

Mohn, J., and others. 2014. Interlaboratory assessment of nitrous oxide isotopomer analysis by isotope ratio mass spectrometry and laser spectroscopy: Current status and perspectives. Rapid Commun. Mass Spectrom. **28**: 1995–2007. doi:10.1002/rcm.6982

Ostrom, N. E., and P. H. Ostrom. 2012. The isotopomers of nitrous oxide: Analytical considerations and application to resolution of microbial production pathways, p. 453–476. *In* M. Baskaran [ed.], Handbook of environmental isotope geochemistry. Advances in isotope geochemistry. Springer. doi:10.1007/978-3-642-10637-8_23

Oswald, K., and others. 2016. Methanotrophy under versatile conditions in the water column of the ferruginous meromictic Lake La Cruz (Spain). Front. Microbiol. **7**:1–16. doi:10.3389/fmicb.2016.01762

Ostrom, N. E., A. Piit, R. Sutka, P. H. Ostrom, A. S. Grandy, K. M. Huizinga, and G. P. Robertson. 2007. Isotopologue effects during N_2O reduction in soils and in pure cultures of denitrifiers. J. Geophys. Res. Biogeo. **112**. doi:10.1029/2006JG000287

Peters, B., K. L. Casciotti, V. A. Samarkin, M. T. Madigan, C. A. Schutte, and S. B. Joye. 2014. Stable isotope analyses of NO_2^-, NO_3^-, and N_2O in the hypersaline ponds and soils of the McMurdo Dry Valleys. Antarctica. Geochim. Cosmochim. Acta **135**: 87–101. doi:10.1016/j.gca.2014.03.024

Ravishankara, A. R., J. S. Daniel, and R. W. Portmann. 2009. Nitrous oxide (N_2O): The dominant ozone-depleting substance emitted in the 21st century. Science **326**: 123–125. doi:10.1126/science.1176985

Risgaard-Petersen, N., S. Rysgaard, and N. P. Revsbech. 1995. Combined microdiffusion-hypobromite oxidation method for determining nitrogen-15 isotope in ammmonium. Soil Sci. Soc. Am. J. **59**: 1077–1080. doi:10.2136/sssaj1995.03615995005900040018x

Robertson, E. K., K. L. Roberts, L. D. W. Burdorf, P. Cook, and B. Thamdrup. 2016. Dissimilatory nitrate reduction to ammonium coupled to Fe(II) oxidation in sediments of a periodically hypoxic estuary. Limnol. Oceanogr. **61**: 365–381. doi:10.1002/lno.10220

Rodrigo, M. A., M. R. Miracle, and E. Vicente. 2001. The meromictic Lake La Cruz (Central Spain). Patterns of stratification. Aquat. Sci. **63**: 406–416. doi:10.1007/s00027-001-8041-x

Santoro, A. E., C. Buchwald, M. R. McIlvin, and K. L. Casciotti. 2011. Isotopic signature of N_2O produced by marine ammonia-oxidizing archaea. Science **333**: 1282–1285. doi:10.1126/science.1208239

Schiff, S. L., J. M. Tsuji, L. Wu, J. J. Venkiteswaran, L. A. Molot, and R. J. Elgood. 2017. Millions of boreal shield lakes can be used to probe Archaean Ocean biogeochemistry. Sci. Rep. **7**: 1–11. doi:10.1038/srep46708

Schreiber, F., P. Wunderlin, K. M. Udert, and G. F. Wells. 2012. Nitric oxide and nitrous oxide turnover in natural and engineered microbial communities: Biological pathways, chemical reactions, and novel technologies. Front. Microbiol. **3**: 1–24. doi:10.3389/fmicb.2012.00372

Sigman, D. M., K. L. Casciotti, M. Andreani, C. Barford, M. Galanter, and J. K. Böhlke. 2001. A bacterial method for the nitrogen isotopic analysis of nitrate in seawater and freshwater. Anal. Chem. **73**: 4145–4153. doi:10.1021/ac010088e

Stanton, C. L., C. T. Reinhard, J. F. Kasting, N. E. Ostrom, J. A. Haslun, T. W. Lyons, and J. B. Glass. 2018. Nitrous oxide from chemodenitrification: A possible missing link in the Proterozoic greenhouse and the evolution of aerobic respiration. Geobiology **16**: 597–609. doi:10.1111/gbi.12311

Stieglmeier, M., M. Mooshammer, B. Kitzler, W. Wanek, S. Zechmeister-Boltenstern, A. Richter, and C. Schleper. 2014. Aerobic nitrous oxide production through N-nitrosating hybrid formation in ammonia-oxidizing archaea. ISME J. **8**: 1135–1146. doi:10.1038/ismej.2013.220

Stookey, L. L. 1970. Ferrozine—A new spectrophotometric reagent for iron. Anal. Chem. **42**: 779–781. doi:10.1021/ac60289a016

Sutka, R. L., N. E. Ostrom, P. H. Ostrom, H. Gandhi, and J. A. Breznak. 2003. Nitrogen isotopomer site preference of N_2O produced by *Nitrosomonas europaea* and *Methylococcus capsulatus* Bath. Rapid Commun. Mass Spectrom. **17**: 738–745. doi:10.1002/rcm.968

Sutka, R. L., N. E. Ostrom, P. H. Ostrom, H. Gandhi, and J. A. Breznak. 2004. Erratum: Nitrogen isotopomer site preference of N_2O produced by *Nitrosomonas europaea* and *Methylococcus capsulatus* Bath. Rapid Commun. Mass Spectrom. **17**: 738–745. doi:10.1002/rcm.968

Sutka, R. L., N. E. Ostrom, P. H. Ostrom, J. A. Breznak, H. Gandhi, A. J. Pitt, and F. Li. 2006. Distinguishing nitrous oxide production from nitrification and denitrification on the basis of isotopomer abundances. Appl. Environ. Microbiol. **72**: 638–644. doi:10.1128/AEM.72.1.638

Tian, H., and others. 2020. A comprehensive quantification of global nitrous oxide sources and sinks. Nature **586**: 248–256. doi:10.1038/s41586-020-2780-0

Tian, Y., C. Xue, C.-Y. Liu, G.-P. Yang, P.-F. Li, W.-H. Feng, and H. W. Bange. 2019. Nitric oxide (NO) in the Bohai Sea and the Yellow Sea. Biogeosciences **16**: 4485–4496. doi:10.5194/bg-16-4485-2019

Toyoda, S., and N. Yoshida. 1999. Determination of nitrogen isotopomers of nitrous oxide on a modified isotope ratio mass spectrometer. Anal. Chem. **71**: 4711–4718. doi:10.1021/ac9904563

Toyoda, S., H. Mutobe, H. Yamagishi, N. Yoshida, and Y. Tanji. 2005. Fractionation of N_2O isotopomers during production by denitrifier. Soil Biol. Biochem. **37**: 1535–1545. doi:10.1016/j.soilbio.2005.01.009

Toyoda, S., N. Yoshida, and K. Koba. 2015. Isotopocule analysis of biologically produced nitrous oxide in various environments. Mass Spectrom. Rev. **36**: 135–160. doi:10.1002/mas

Trimmer, M., P.-M. Chronopoulou, S. T. Maanoja, R. C. Upstill-Goddard, V. Kitidis, and K. J. Purdy. 2016. Nitrous oxide as a function of oxygen and archaeal gene abundance in the North Pacific. Nat. Commun. **7**: 1–10. doi:10.1038/ncomms13451

Venterea, R. T. 2007. Nitrite-driven nitrous oxide production under aerobic soil conditions: Kinetics and biochemical controls. Glob. Chang. Biol. **13**: 1798–1809. doi:10.1111/j.1365-2486.2007.01389.x

Vicente, E., and M. R. Miracle. 1988. Physicochemical and microbial stratification in a meromictic karstic lake of Spain. SIL Proceedings **1922–2010**: 522–529. doi:10.1080/03680770.1987.11897974

Visser, A., S. D. Wankel, P. A. Niklaus, J. M. Byrne, A. A. Kappler, and M. F. Lehmann. 2020. Impact of reactive surfaces on the abiotic reaction between nitrite and ferrous iron and associated nitrogen and oxygen isotope dynamics. Biogeosciences **17**: 4355–4374. doi:10.5194/bg-17-4355-2020

Walter, X. A. 2011. Anaerobic iron cycling in a neoarchean ocean analogue. Ph.D. thesis. Université de Neuchâtel.

Walter, X. A., A. Picazo, M. R. Miracle, E. Vicente, A. Camacho, M. Aragno, and J. Zopfi. 2014. Phototrophic Fe(II)-oxidation in the chemocline of a ferruginous meromictic lake. Front. Microbiol. **5**:1–9. doi:10.3389/fmicb.2014.00713

Wang, W. C., Y. L. Yung, A. A. Lacis, T. Mo, and J. E. Hansen. 1976. Greenhouse effects due to man-made pertubations of trace gases. Science **194**: 685–690. doi:10.1126/science.194.4266.685

Wankel, S. D., W. Ziebis, C. Buchwald, C. Charoenpong, J. D. Di. De Beer, Z. Xu, and K. Zengler. 2017. Evidence for fungal and chemodenitrification based N_2O flux from nitrogen impacted coastal sediments. Nat. Commun. **8**: 1–11. doi:10.1038/ncomms15595

Weiss, R. F., and B. A. Price. 1980. Nitrous oxide solubility in water and seawater. Mar. Chem. **8**: 347–359. doi:10.1016/0304-4203(80)90024-9

Wenk, C. B., C. H. Frame, K. Koba, and others. 2016. Differential N_2O dynamics in two oxygen-deficient lake basins revealed by stable isotope and isotopomer distributions. Limnol. Oceanogr. **61**: 1735–1749. doi:10.1002/lno.10329,

Westley, M. B., H. Yamagishi, B. N. Popp, and N. Yoshida. 2006. Nitrous oxide cycling in the Black Sea inferred from stable isotope and isotopomer distributions. Deep. Res. Part II Top. Stud. Oceanogr. **53**: 1802–1816. doi:10.1016/j.dsr2.2006.03.012

Wrage, N., G. L. Velthof, M. L. Van Beusichem, and O. Oenema. 2001. Role of nitrifier denitrification in the production of nitrous oxide. Soil Biol. Biochem. **33**: 1723–1732. doi:10.1016/S0038-0717(01)00096-7

Yamagishi, H., M. B. Westley, B. N. Popp, S. Toyoda, N. Yoshida, S. Watanabe, K. Koba, and Y. Yamanaka. 2007. Role of nitrification and denitrification on the nitrous oxide cycle in the eastern tropical North Pacific and Gulf of California. J. Geophys. Res. Biogeo. **112**:1–15. doi:10.1029/2006JG000227

Yamazaki, T., T. Hozuki, K. Arai, S. Toyoda, K. Koba, T. Fujiwara, and N. Yoshida. 2014. Isotopomeric characterization of nitrous oxide produced by reaction of enzymes extracted from nitrifying and denitrifying bacteria. Biogeosciences **11**: 2679–2689. doi:10.5194/bg-11-2679-2014

Yoshida, N. 1988. ^{15}N-depleted N_2O as a product of nitrification. Nature **355**: 528–529. doi:10.1038/335528a0

Yoshida, N., and S. Toyoda. 2000. Constraining the atmospheric N_2O budget from intramolecular site preference in N_2O isotopomers. Nature **405**: 330–334. doi:10.1038/35012558

Zhang, L., M. A. Altabet, T. Wu, and O. Hadas. 2007. Sensitive measurement of NH_4^+ $^{15}N/^{14}N$ ($\delta^{15}NH_4^+$) at natural abundance levels in fresh and saltwaters. Anal. Chem. **79**: 5297–5303. doi:10.1021/ac070106d

Zhu, X., M. Burger, T. A. Doane, and W. R. Horwath. 2013. Ammonia oxidation pathways and nitrifier denitrification are significant sources of N_2O and NO under low oxygen availability. PNAS **110**: 6328–6333. doi:10.1073/pnas.1219993110

Zopfi, J., M. E. Böttcher, and B. B. Jørgensen. 2008. Biogeochemistry of sulfur and iron in Thioploca-colonized surface sediments in the upwelling area off Central Chile. Geochim. Cosmochim. Acta **72**: 827–843. doi:10.1016/j.gca.2007.11.031

Acknowledgments

Thomas Kuhn is thanked for his great efforts in keeping the IRMS up and running. Jessica Venetz is thanked for her help in the field, as well as in the laboratory, and Joachim Mohn (EMPA) is acknowledged for calibrating and providing N_2O isotope standards. We highly appreciate the helpful comments of three anonymous reviewers. This study was funded by the Swiss National Science Foundation project 153055 granted to J.Z. and M.F.L. Open access funding was provided by the University of Basel.

Conflict of Interest

None declared.

Submitted 05 November 2021
Revised 11 March 2022
Accepted 22 May 2022

Associate editor: Werner Eckert